Turkish Journal of Electrical Engineering & Computer Sciences

http://journals.tubitak.gov.tr/elektrik/

Research Article

Turk J Elec Eng & Comp Sci
(2019) 27: 4541 – 4550

doi:10.3906/elk-1901-167

A hybrid multiband printed loop antenna for WLAN/WiMAX bands for applications in MIMO systems

Sayed Ali SHAHSHAHANI, Mohammad Amin HONARVAR*
Department of Electrical Engineering, Najafabad Branch, Islamic Azad University, Najafabad, Iran

Received: 23.01.2019 • **Accepted/Published Online:** 19.06.2019 • **Final Version:** 26.11.2019

Abstract: In this article a thin hybrid multiband printed loop antenna is presented for application in multiple-input multiple-output (MIMO) systems. The proposed antenna has several advantages; for example, the pseudofilter feature of the proposed antenna is one of this antenna's advantages. Because of the antenna's width (9.5 mm), it can be used on the edges of the board. The first resonant frequency is generated by the original loop of the antenna. Incorporation of different embedded components, i.e. a subsidiary loop, extended ground-traces, parasitic patch, and the slits, results in the proposed antenna resonating as a multiband antenna. This antenna is adjusted in such a way that it resonant in WLAN (2.4, 5.2, and 5.8 GHz) and WiMAX (3.5 GHz) bands. Four antennas are used as a MIMO system that are sequentially and perpendicularly placed along the edges of the board. In conclusion, the antenna design is confirmed according to simulation results obtained from the constructed prototype and associated measuring results.

Key words: Printed antenna, loop antenna, multiband, MIMO systems

1. Introduction

In recent years, there has been a significant increase in the demand for high-speed and high-quality data transmission in wireless communications, making multiple-input multiple-output (MIMO) technology highly desirable. MIMO technology has excellent performance in terms of channel capacity without occupying extra spectrum and radiation power by transmitting several separate data streams simultaneously. Most of the wireless local area network (WLAN) and Worldwide Interoperability for Microwave Access (WiMAX) devices use MIMO technology in receiver or transmitter antennas. In these systems, in addition to increasing the rate of data transfer, fading effect, reliability, and signal quality are also improved.

A practical MIMO antenna should have a low signal correlation between the antenna elements and efficient matching characteristics of the input impedance [1]. The mutual coupling in multiple antennas is largely related to the surface-current coupling [2, 3]. In [4], a new set of antennas perpendicular to each other was designed to reduce mutual correlation of multiple antennas. Thus, the multiple antennas become capable of obtaining more isolation when the fields of the antennas are perpendicular to each other. To mitigate large coupling between the antenna elements operating on the same frequency bands, development of loop antennas is a very promising solution. A self-balanced, one-wavelength loop antenna would be particularly beneficial [5] due to its capabilities for exciting fewer surface currents on the system or on the antenna ground plane.

With the rapid development of modern wireless communication systems, antenna design has focused mainly on multiband functionality coupled with simplified and miniature structures that can be easily fabricated.

*Correspondence: amin.honarvar@pel.iaun.ac.ir

Due to the small size and low cost of such systems, there has been a surge of interest [4] in printed antennas. To cover multiple bands simultaneously, various antennas including a multiple mode monopole antenna, loop, and slot antenna have been proposed [4–15]. However, classic loop antennas are typically narrow band radiators that occupy much space. Wideband antennas with loop-split-ring resonator (SRR) composite structures and hybrid loops were reported in [12] and [13], respectively. Printed loop antennas have been widely used in laptop computers and mobile phones [13, 14]. Their geometrical configurations are thin and rectangular, with a long length-to-width ratio. In order to reduce or eliminate the system ground plane effects on antenna performance, modified one-wavelength loop antennas have been proposed. Furthermore, two planar asymmetric loops, to enhance the operating impedance bandwidth of the antenna, have been reported [15].

In this paper, a thin hybrid multiband printed loop antenna operating across WLAN (2.4, 5.2, and 5.8 GHz) and WiMAX (3.5 GHz) systems without extra bands is proposed. The independence of resonant frequencies in the proposed antenna is achieved by adjusting all the frequency bands of the antenna without changing the structure of the resonators. The thickness of the proposed antenna is also suitable for the edges of the board; thus, the antenna is used for constructing a four-element MIMO system. The proposed antenna achieved mutual coupling isolation of -23 dB without decoupling the structure. Finally, the results obtained from the simulation of the proposed antenna are compared with those resulting from the constructed prototype. The measured characteristics of the prototype confirmed the simulation results.

2. Antenna design considerations

In this section, we present different design aspects of the proposed antenna. Figure 1 illustrates the geometry of the proposed multiband hybrid antenna, which includes a main loop and a subsidiary loop with extended ground-traces and a parasitic patch with an embedded slit. The whole circumference of the loops is close to one wavelength of the frequency at the base resonance. By properly choosing the dimensions, the proposed antenna covers WLAN and WiMAX operation bands, which is successfully achieved with an antenna dimension of 9.5×41 mm^2. The proposed antenna was fabricated on a substrate of glass-reinforced epoxy laminate material (FR4) with $\mu_r = 4.3$ and a thickness of 1.6 mm.

To better illustrate the performance of the proposed antenna, the simulated return loss (S_{11}) is shown in Figure 2. The impedance bandwidth of $S_{11} < -10$ dB is observed to cover four bands at 2.465 GHz (2.30–2.57), 5.255 GHz (5.13–5.36), and 5.775 GHz (5.69–5.87) for utilization in WLAN systems and 3.545 GHz (3.39–3.74) for use in WiMAX systems.

Antenna analyses were conducted by investigating the surface current distribution at the antenna's resonant frequencies. The surface current of the antenna is shown at a frequency of 2.465 GHz (Figure 3a). The resonance at this frequency is due to excitement of the first unbalanced mode of the main loop. The electrical length of the loop circumference is half of the wavelength at a frequency of 2.465 GHz with one surface current null. The antenna's main loop dimensions are approximately expressed by $2.Lsl+2.Wsl-Upo \approx \frac{\lambda_1}{2} = 60.85$ mm at $f_1 = 2.465$ GHz. Figure 3b shows the surface current distribution at a frequency of 3.545 GHz. This resonant frequency is due to the coupling surface current of the main loop on the parasitic patch. The length of the parasitic patch is approximately defined by $Lp \approx Lsl \approx \frac{\lambda_2}{4} = 21.15$ mm at $f_2 = 3.545$ GHz. Figure 3c shows the antenna surface current distribution at 5.255 GHz. The coupling surface current of the main loop on the parasitic patch causes a circular current around the slit on the patch, which causes resonance of the structure at 5.255 GHz. The length of the slit on the parasitic patch is approximately calculated by $2.Ls \approx \frac{\lambda_3}{4} = 14.27$ mm

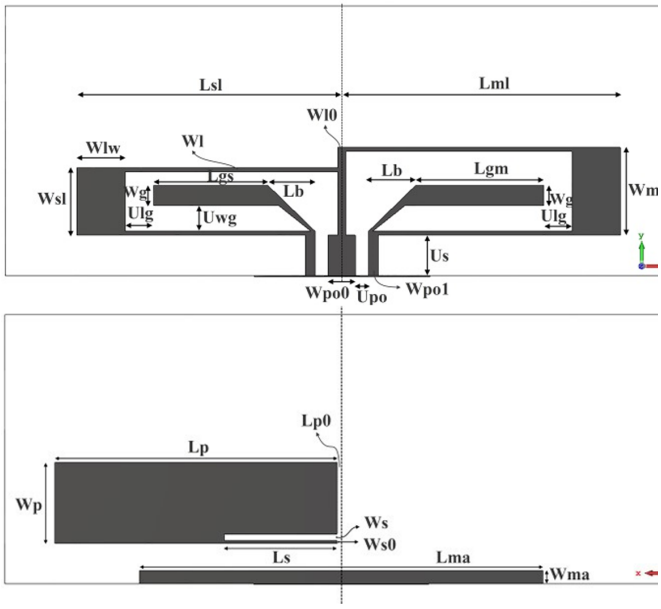

Figure 1. Geometry and dimensions of the proposed antenna.

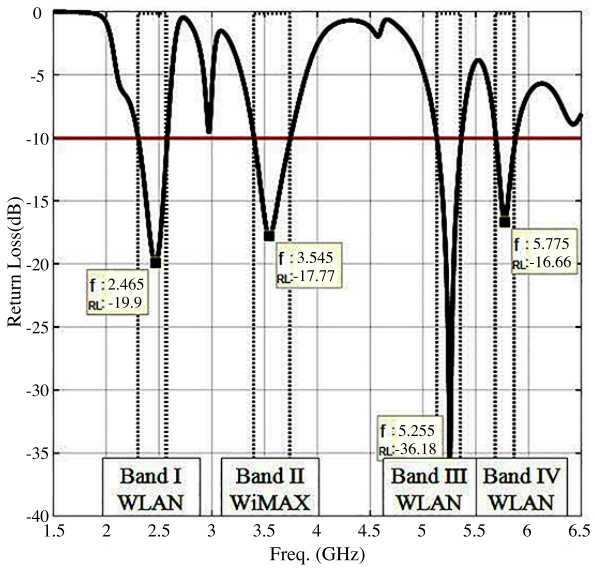

Figure 2. Simulated return loss of proposed antenna.

at $f_3 = 5.255$ GHz. Finally, Figure 3d shows the antenna surface current at 5.775 GHz. The excitation at this frequency is due to the incitement of the second unbalanced mode of the main loop, which has two surface current nulls. The loop circumference is equal to the wavelength at 5.775 GHz. The extended ground-traces cause a shorter path and effect on the electrical length of the loop in this mode. It can be approximated by $2.Wsl + 2.Lsl - Upo - Ulg \approx \lambda_4 = 51.948$ mm at $f_4 = 5.775$ GHz for the extended ground-trace parameters.

In order to analyze the structural parts of the proposed antenna, their effects on the return loss of the antenna have been investigated. By removing the subsidiary loop shown in Figure 4a, resonant frequency decreases in the first and the second modes of the loop. This behavior is observed because of the existence of a parasitic patch behind the main loop leading to a sharp decrease in the magnetic field of the loop. Resonance reduction at 3.5 and 5.2 GHz is due to the removal of the subsidiary loop that omitted the coupling surface current on the parasitic patch resulting in inappropriate impedance matching. Without the extended ground-traces (Figure 4b), resonant frequencies at 5.8 GHz and 4.6 GHz will shift to 5.4 GHz and 4.4 GHz, respectively. Due to the impedance matching at 4.4 GHz, this resonance will cause inappropriate radiation. Also, it is worth mentioning that the extra resonance related to the surface current of the sharp edges of the extended ground-traces is eliminated at 3 GHz. Removing the slit embedded in the parasitic patch (Figure 4c) would eliminate the circulation current exciting the resonance at 5.2 GHz. It would excite the undesirable high-order mode resonant frequency at 4.6 GHz. By removing the parasitic patch (Figure 4d), the resonance at 3.5 GHz and 5.2 GHz produced by the slit on the parasitic patch was eliminated. The return loss of the main structure along with the return loss of structures are sequentially shown in Figure 4e.

Most of the parameters changing the first resonance of the antenna brought about a change in the fourth resonant frequency of the antenna due to its second unbalanced mode of the loop. After adjusting the first resonant frequency, however, the fourth resonant frequency can be adjusted by changing Wlw (step line width) independently. The second resonant frequency is related to the dimensions of the parasitic patch. Furthermore,

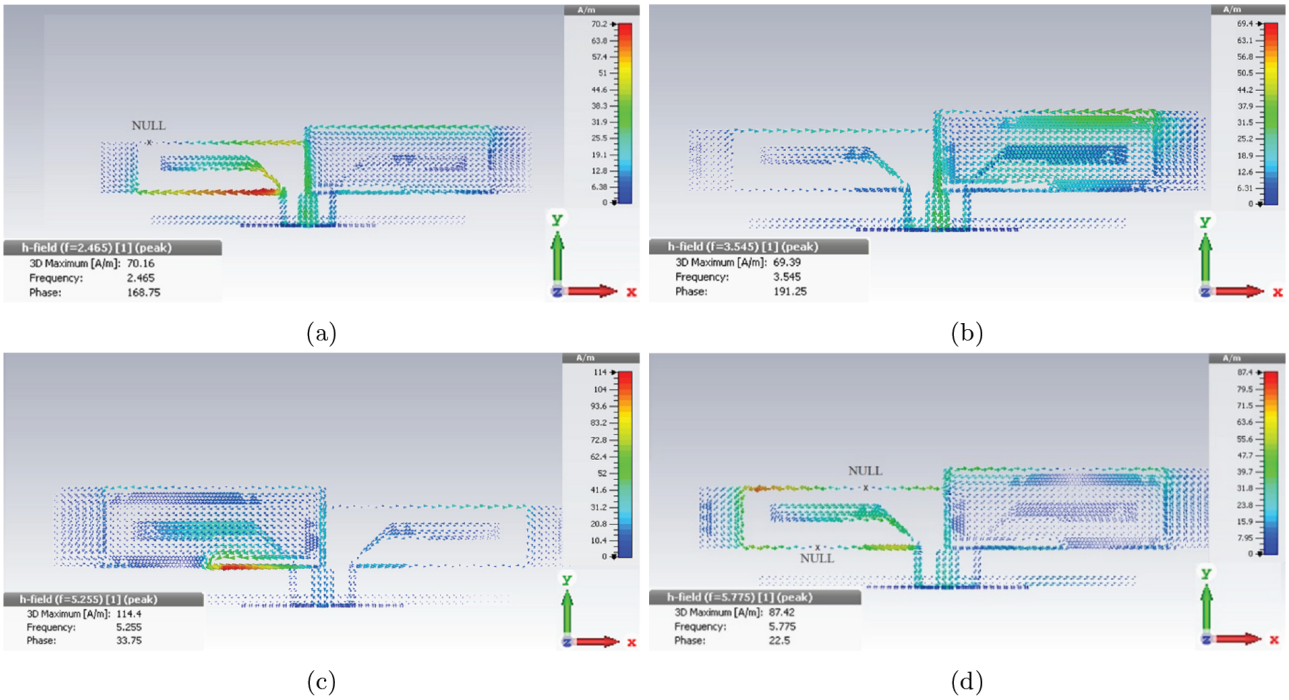

Figure 3. Surface current distribution of the proposed antenna at (a) 2.465 GHz, (b) 3.545 GHz, (c) 5.255 GHz, and (d) 5.775 GHz.

Table 1. Dimensions for the proposed antenna (diam. in mm).

$Ws0 = 0.2$	$Wg = 1.5$	$Ulg = 2.1$	$Lp = 21$	$Lsl = 19.7$
$Wma = 1$	$Lgs = 8.5$	$Us = 3$	$Wp = 6$	$Wsl = 5$
$Lma = 30$	$Lgm = 9.5$	$Wpo0 = 2$	$Lp0 = 0.3$	$Wl0 = 0.6$
$Lml = 20.7$	$Lb = 3.5$	$Wpo1 = 0.7$	$Ws = 0.5$	$Wl = 0.3$
$Wml = 6.5$	$Uwg = 1.9$	$Upo = 1$	$Ls = 8.4$	$Wlw = 3.6$

the third resonant frequency is related to the slit length on the parasitic patch. These resonant frequencies were adjusted independently of other resonant frequencies. It was observed that the proposed antenna was capable of adjusting the frequency and the resonant frequency bands independently. The preferred dimensions of the proposed multiband antenna are shown in Table 1. These dimensions were computed by parametric optimization assisted by Computer Simulation Technology (CST) software.

3. Results and discussion

In this section, simulation and experimental results are presented to evaluate the performance of the proposed antenna.

3.1. S-parameters

Figure 5 shows the photograph of a prototype antenna for a better understanding of its dimensions from the top to the bottom layers of the substrate. Characteristics of the prototype antenna were measured with an

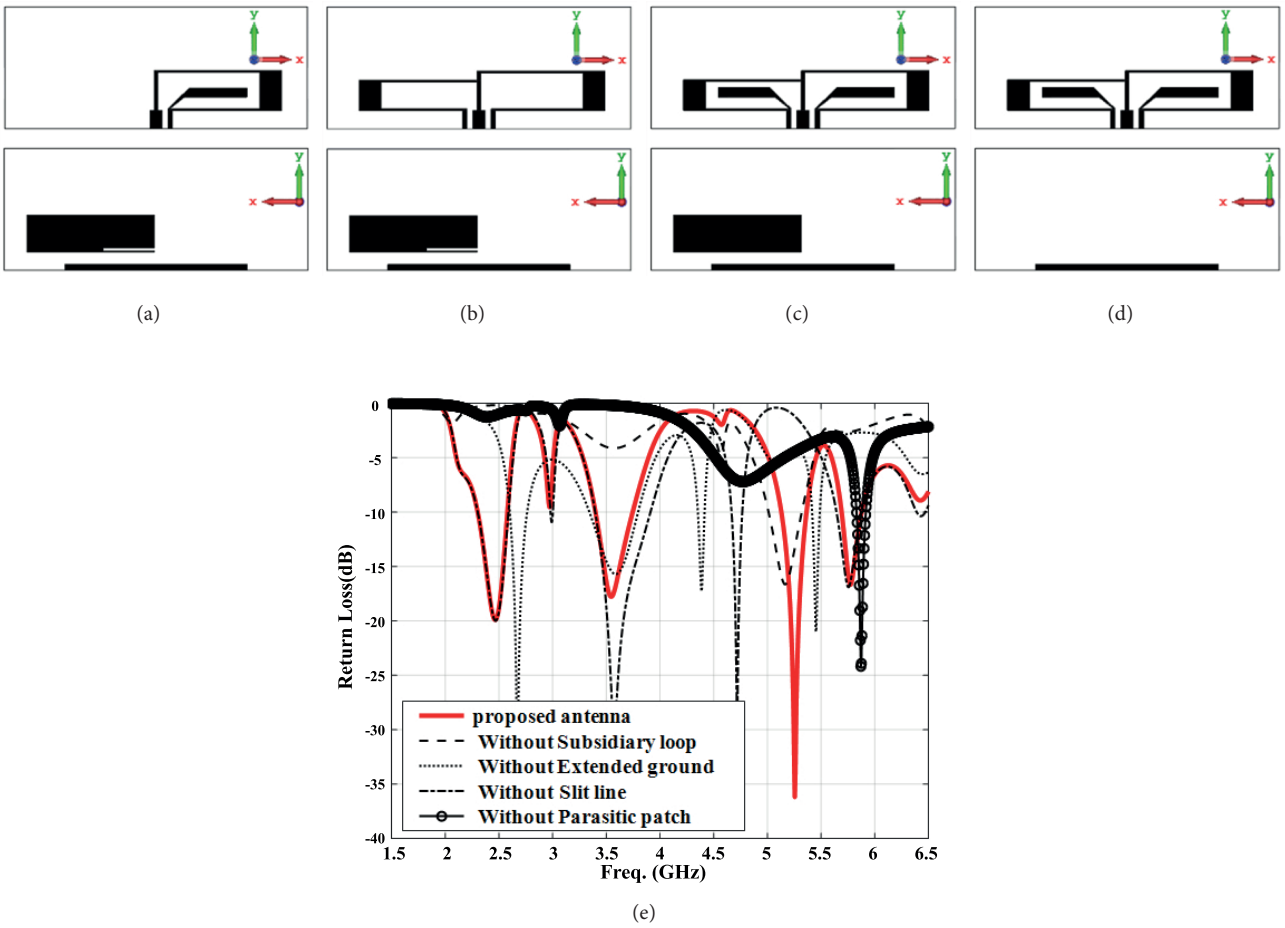

Figure 4. Structure of the proposed antenna without: (a) subsidiary loop, (b) extended ground-traces, (c) slit on patch, (d) parasitic patch, (e) return loss of proposed antenna with/without structures.

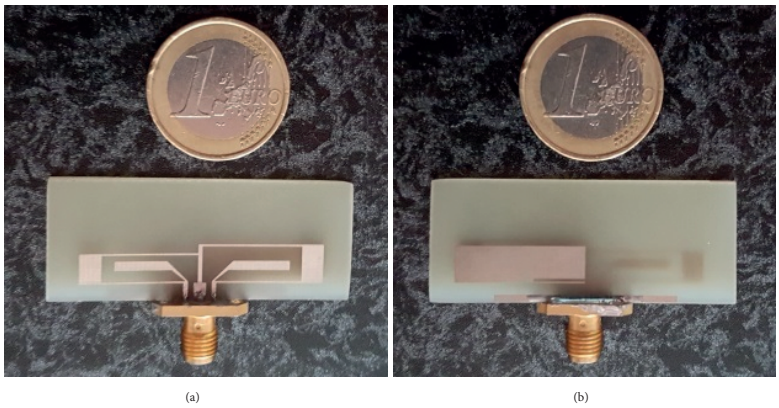

Figure 5. (a) Top layer and (b) bottom layer of the proposed prototype antenna.

Agilent 8722ES S-parameter network analyzer.

Figure 6 shows comparison results between the simulated and the measured return loss of the prototype

antenna. The antenna operates at the frequency ranges of 2.21–2.7 GHz, 5.35–5.5 GHz, and 5.65–5.85 GHz to cover the bands of WLAN and 3.4–3.95 GHz to cover WiMAX systems. The measured center frequency of the second WLAN band slightly shifts up from the simulated results. These results exhibit acceptable overall agreement between the simulated and prototype systems, except for some losses that can be attributed to the ideal simulation characteristics of the substrate and also due to the difference in the structure of the input SMA port. The prototype antenna was appropriately resonated around the designed frequencies.

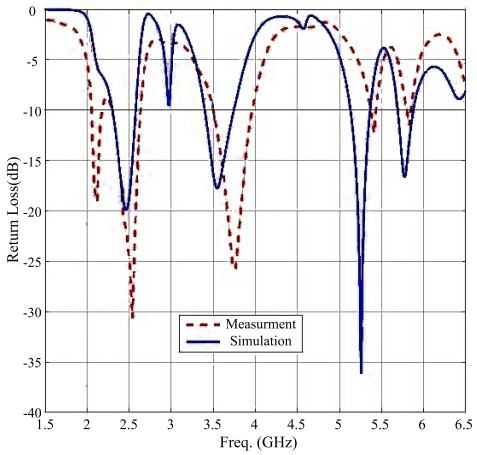

Figure 6. Measured and simulated return loss of the proposed antenna.

3.2. Integration with a four-element MIMO antenna

Figure 7 illustrates the return loss, isolation diagram, and location of the proposed antenna incorporated with the structure of a four-element MIMO antenna. Every two antennas located beside each other are mutually perpendicular in the proposed MIMO structure to reduce potential correlations between them. The distance between two close antennas is 0.36λ (at 2.465 GHz). The size of the entire structure is suitable to be used in normal wireless systems. In particular, due to the structure of the antenna being thin and along the edge, it only occupies limited space and leaves room for the other circuit's elements and electronic components of the wireless system. It is observed that the characteristics of each of the four antennas are consistent with those of the proposed antenna. In addition, in case the two antennas are perpendicular, the mutual coupling of the antennas is reduced to a suitable level of -23 dB.

3.3. Diversity performance

The isolation rate of the antennas in MIMO systems is based on the correlation of antennas to each other. We calculate the envelope correlation coefficient (ECC) of two possible states of parallel and perpendicular relations between two antennas based on the return loss of the proposed antenna [12] as follows:

$$\text{Perpendicular mode:} \quad \rho_{e1} = \frac{|S_{11}^* S_{12} + S_{12}^* S_{22} + S_{13}^* S_{32} + S_{14}^* S_{42}|^2}{(1-(|S_{11}|^2+|S_{21}|^2+|S_{31}|^2+|S_{41}|^2))(1-(|S_{12}|^2+|S_{22}|^2+|S_{32}|^2+|S_{42}|^2))}, \tag{1}$$

and

$$\text{Parallel mode:} \quad \rho_{e2} = \frac{|S_{11}^* S_{13} + S_{12}^* S_{23} + S_{13}^* S_{33} + S_{14}^* S_{43}|^2}{(1-(|S_{11}|^2+|S_{21}|^2+|S_{31}|^2+|S_{41}|^2))(1-(|S_{13}|^2+|S_{23}|^2+|S_{33}|^2+|S_{43}|^2))}. \tag{2}$$

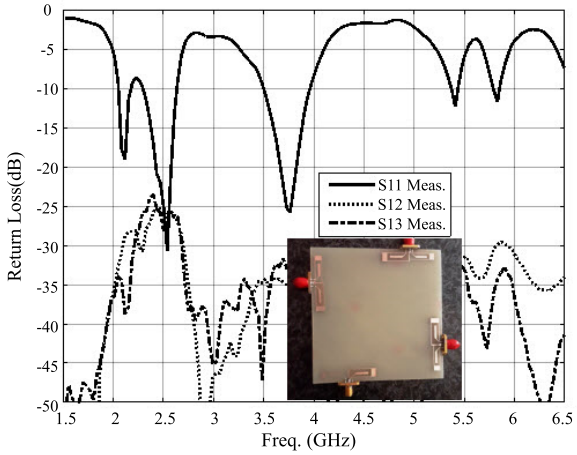

Figure 7. Isolation of measured MIMO antenna.

Figure 8 illustrates the correlation coefficient of the proposed antenna incorporated with the MIMO system for antennas in both parallel and perpendicular positions. The maximum correlation coefficient of the antennas is less than 0.09, which is suitable for MIMO antennas. Besides, based on the calculated results, the envelope correlation values of less than 0.009 remain within the bands of interest, which is much better than the value of 0.3 required based on industrial specifications. The proposed MIMO antenna achieves significant reduction in ECC, which means that the proposed antenna has a good isolation performance.

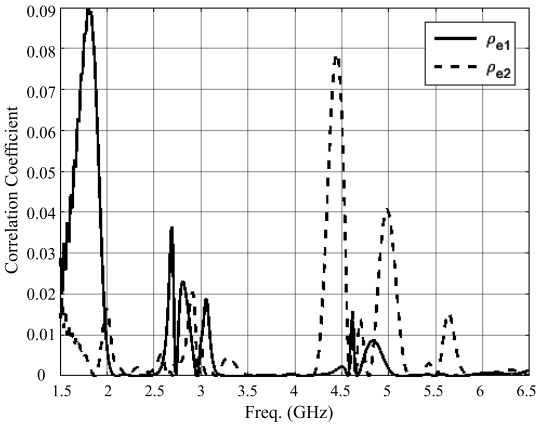

Figure 8. Envelope correlation coefficient of simulated MIMO antenna.

Also, in order to assess the diversity performance of the proposed MIMO antenna, some important parameters are evaluated using a 3D radiation pattern method [16] and summarized in Table 2, including the isolation between parallel and perpendicular antennas, mean effective gain (MEG), diversity gain (DG), and envelope correlation coefficient ρ_{e2}.

3.4. Gain, efficiency, and radiation patterns

Figure 9 shows the gain and efficiency of the proposed antenna at the operating frequencies. Despite the low gain of microstrip antennas, the proposed antenna has a proper range of 2.5–4.12 dBi gain and 88.9%–90.9% efficiency.

Table 2. Diversity performance of the proposed MIMO antenna.

Frequency (GHz)	Isolation perpendicular (dB)	Isolation parallel (dB)	$MEG_{1,2,3}$ (Γ=6 dB)	Diversity gain (dB)	ρ_{e2} (Parallel mode)
2.465	−24.40	−18.55	−4.511	9.993	0.0000136
3.545	−33.52	−25.42	−4.672	9.999	0.0000082
5.255	−32.63	−15.42	−4.191	9.999	0.00000064
5.775	−28.63	−17.39	−3.879	9.999	0.0000079

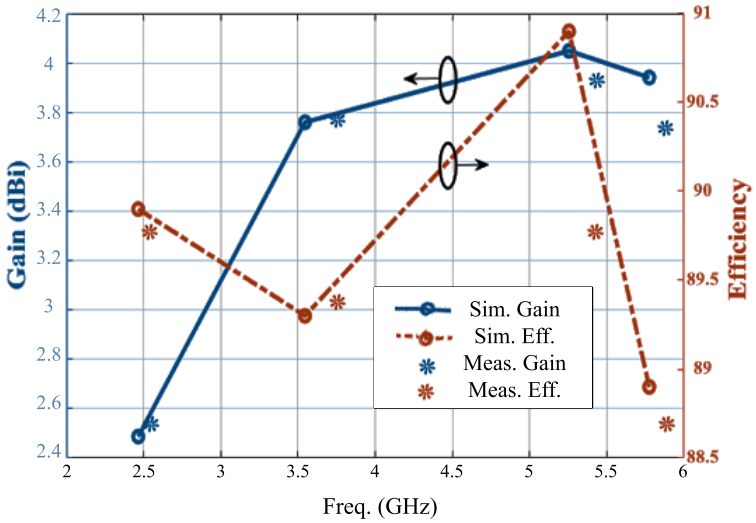

Figure 9. Gain and efficiency of the proposed antenna.

The normalized radiation pattern of the proposed antenna is shown in Figure 10 at different operating frequencies. Due to use of structures with similar radiation patterns, the proposed antenna pattern at all operating frequencies is similar to that of the loop antenna. This pattern of homology, which is a desirable feature for antennas, leads to the stability of radiation of the antenna at resonant frequencies. The asymmetric radiation pattern may be caused by the unbalanced feed and nonuniform current distribution along the circular loops. Moreover, more variations and nulls in the radiation patterns can be seen for frequencies in the higher operation band.

Comparisons of the proposed antenna and recently reported MIMO antennas [1, 3, 5, 11, 13] in terms of isolation structure, number of frequency bands and MIMO antennas, antenna distance, size, and isolation are listed in Table 3. The results show that the proposed antenna with narrow size and satisfying isolation is a good candidate for MIMO system applications.

4. Conclusion

A multiband thin printed loop antenna was designed and simulated for use in WLAN systems (2.4, 5.2, and 5.8 GHz) and WiMAX (3.5 GHz). Frequency independence and removal of the extra frequency spectrum were investigated. The proposed antenna is suitable for the edges of wireless systems. Due to the thinness of the antenna and dimensions of the wireless devices, the proposed antenna can be used for four-antenna MIMO systems. The prototype of the simulated antenna was implemented and also tested.

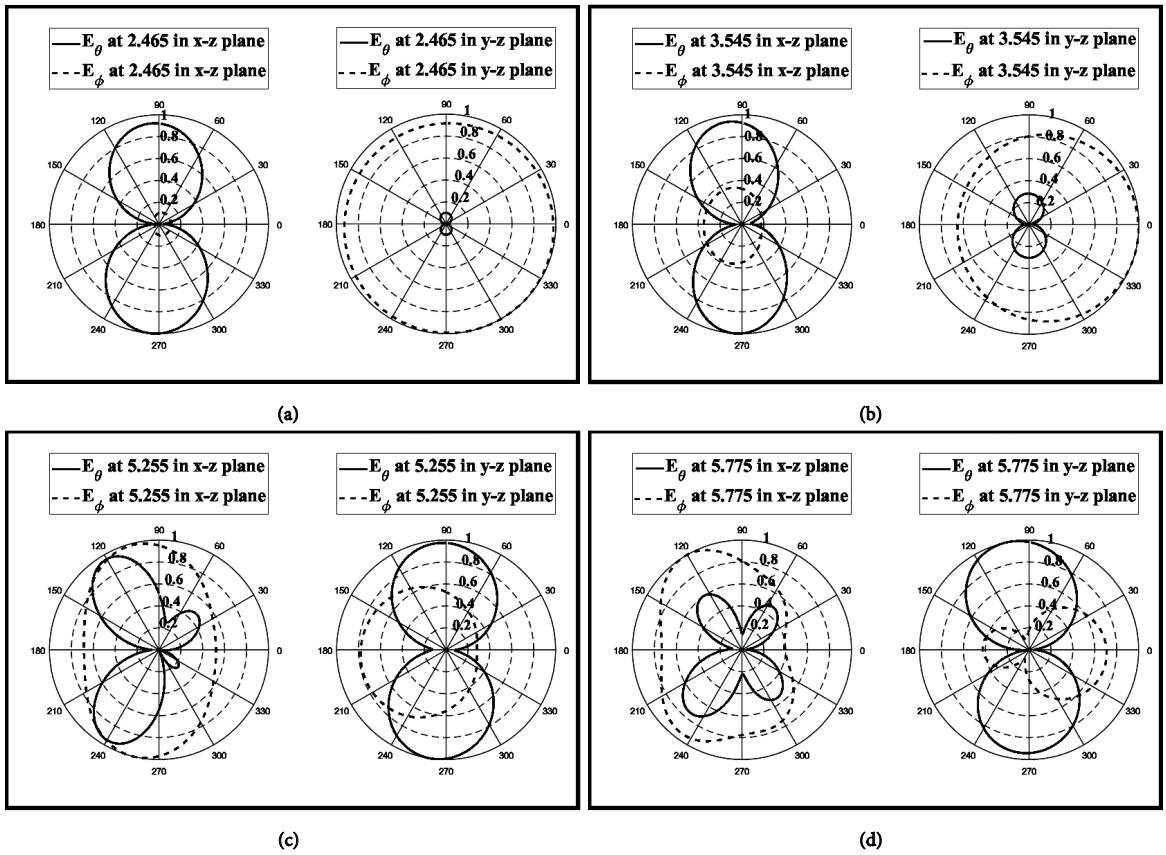

Figure 10. Radiation pattern of proposed antenna at (a) 2.465 GHz, (b) 3.545 GHz, (c) 5.255 GHz, and (d) 5.775 GHz.

Table 3. Performance comparisons of the proposed and reference antennas.

Reference	Size of antenna (mm^3)	Frequency band number	Isolation structure	Num. of antennas	Antenna distance	Isolation (dB)
Ref. [1]	$22 \times 29 \times 0.78$	1	Yes	2	$0.1\lambda_0$	−16
Ref. [3]	$45 \times 55 \times 0.8$	1	Yes	2	$0.3\lambda_0$	−21.6
Ref. [5]	$20 \times 40 \times 10$	3	Yes	3	$0.34\lambda_0$	−15
Ref. [11]	$28.5 \times 28.5 \times 1.6$	1	Yes	4	$0.15\lambda_0$	−20
Ref. [13]	$31 \times 13 \times 0.8$	3	Yes	2	$0.1\lambda_0$	−13
Proposed antenna	$9.5 \times 41 \times 1.6$	4	No	4	$0.36\lambda_0$	−16

References

[1] Malekpour N, Honarvar MA, Dadgarpur A, Virdee BS, Denidni TA. Compact UWB mimo antenna with band-notched characteristic. Microwave and Optical Technology Letters 2017; 56 (5): 1037-1041. doi: 10.1002/mop.30462

[2] Nirmal P, Nandgaonka AB, Sanjay LN. A MIMO antenna: study on reducing mutual coupling and improving isolation. In: Recent Trends in Electronics, Information & Communication Technology; Bangalore, India; 2016. pp. 1736-1740. doi: 10.1109/RTEICT.2016.7808131

[3] Al-Fayyadh HQ, Abdulhameed AA. Flexible (2×1) MIMO antenna with electromagnetic band gap unit cell for WiMAX applications. Turkish Journal of Electrical Engineering and Computer Science 2017; 25 (4): 3061-3072.

doi: 10.3906/elk-1603-94

[4] Karimian R, Oraizi H, Fakhte S, Farahani M. Novel F-shaped quad-band printed slot antenna for wlan andwimaxmimo systems. IEEE Antennas and Wireless Propagation Letters 2013; 12: 405-408. doi: 10.1109/LAWP.2013.2252140

[5] Su SW. High-gain dual-loop antennas for MIMO access points in the 2.4/5.2/5.8 GHz bands. IEEE Transactions on Antennas and Propagation 2010; 58 (7): 2412-2419. doi: 10.1109/TAP.2010.2048871

[6] Malik JS, Rafique U, Ali SA, Khan MA. Novel patch antenna for multiband cellular, WiMAX, and WLAN applications. Turkish Journal of Electrical Engineering and Computer Science 2017; 25: 2005-2014. doi: 10.3906/elk-1512-83

[7] Honarvar MA, Hamidi N, Virdee BS. Multiband antenna for portable device pplications. Microwave and Optical Technology Letters 2015; 57 (4): 956-959. doi: 10.1002/mop.28994

[8] Palandöken M . Dual broadband antenna with compact double ring radiators for IEEE 802.11 ac/b/g/n WLAN communication applications. Turkish Journal of Electrical Engineering and Computer Science 2017; 25: 1326-1333. doi: 10.3906/elk-1507-121

[9] Desai A, Upadhyaya T, Palandöken M. Dual band slotted transparent resonator for wireless local area network applications. Microwave and Optical Technology Letters 2018; 60 (12): 3034-3039. doi: 10.1002/mop.31417

[10] Kaya A, Baytre C, Palandöken M, Kaya I, Ozbakis B. A dual-band MIMO monopole antenna system for set top box and WLAN chipsets. In: Proceedings of the 2nd World Congress on Electrical Engineering and Computer Systems and Science; Budapest, Hungary; 2016. p. 140. doi:10.11159/eee16.140

[11] Wenjing W, Bo Y, Aiting W. A quad-element UWB-MIMO antenna with band-notch and reduced mutual coupling based on EBG structures. International Journal of Antennas and Propagation 2018; 2018: 1-10. doi: 10.1155/2018/8490740

[12] Xu K, Liu F, Peng L, Zhao WS, Ran L et al. Multimode and wideband printed loop antenna based on degraded split-ring resonators. IEEE Access 2017; 5: 15561-15570. doi: 10.1109/ACCESS.2017.2729517

[13] Zhu J, Feng B, Peng B, Deng L, Li S. Multiband printed mobile MIMO antenna for WWAN and LTE applications. Microwave and Optical Technology Letters 2017; 59 (6): 1446-1450. doi: 10.1002/mop.30567

[14] Chiu CW, Chi YJ. Printed loop antenna with a U-shaped tuning element for hepta-band laptop applications. IEEE Transactions on Antennas and Propagation 2010; 58 (11): 3464-3470. doi: 10.1109/TAP.2010.2071343

[15] Peng CM, Chen IF, Yeh JW. Printed broadband asymmetric dual-loop antenna for WLAN/WiMAX applications. IEEE Antennas and Wireless Propagation Letters 2013; 12: 898-901. doi: 10.1109/LAWP.2013.2273231

[16] Yuan D, Zhengwei D, Ke G, Zhenghe F. A novel dual-band printed diversity antenna for mobile terminals. IEEE Transactions on Antennas and Propagation 2007; 55 (7): 2088-2096. doi:10.1109/TAP.2007.900249